Cell. Mol. Biol. (ISSN: 1165-158X)

Journal Homepage: www.cellmolbiol.org

Cellular and Molecular Biology

Original Article

LINC01232 regulates miR-516a-5p/BCL9 axis to promote triple-negative breast cancer progression

Wei Liu[1], Yunfeng Niu[2], Jie An[2*]

[1] Department of General Surgery, Bethune International Peace Hospital, No. 398 Zhongshan West Road, Qiaoxi District, Shijiazhuang, Hebei, China
[2] Department of Pathology, Bethune International Peace Hospital, No. 398 Zhongshan West Road, Qiaoxi District, Shijiazhuang, Hebei, China

Article Info

Article history:

Received: March 29, 2025
Accepted: June 19, 2025
Published: July 31, 2025

Use your device to scan and read the article online

Abstract

Triple-negative breast cancer (TNBC) is characterised by an absence of the oestrogen receptor (ER), progesterone receptor (PR) and human epidermal growth factor receptor 2 (HER2), for which there are few therapeutic options and the prognosis is poor. This research sought to explore the particular function of the long non-coding RNA (lncRNA) LINC01232 in TNBC and its regulatory impacts on the miR-516a-5p/BCL9 pathway. In this study, quantitative reverse transcription polymerase chain reaction (qRT-PCR) was used to determine the expression level of LINC01232 in TNBC tissues. We also examined its regulatory influences on miR-516a-5p and BCL9 via cellular function tests and a luciferase reporter experiment. Evaluated the effect of LINC01232 silencing on proliferation, migration and invasion of breast cancer cells. Results showed that LINC01232 expression was abnormally high in TNBC tissues in comparison to normal tissues. Inhibition of LINC01232 expression markedly impeded breast cancer cell proliferation, clone formation, migration and invasion. We found that LINC01232 competes with miR-516a-5p for binding, thereby reducing its expression and subsequently increasing BCL9 expression. In conclusion, our results indicate that LINC01232 facilitates the malignant development of TNBC through the miR-516a-5p/BCL9 pathway, providing fresh perspectives on the pathogenesis of TNBC and pinpointing potential therapeutic targets.

Keywords: LINC01232, miR-516a-5p, BCL9, Triple-negative breast cancer, ceRNA.

1. Introduction

Triple-negative breast cancer (TNBC) is identified by the lack of expression of estrogen receptor (ER), progesterone receptor (PR), and human epidermal growth factor receptor 2 (HER2)[1]. TNBC represents 10.0%-20.8% of all breast cancer patients. It stands out due to its distinct biological characteristics, clinicalopathological traits, and less favorable outcomes as compared to other subtypes of breast cancer[2]. The 5-year survival rate for patients with early TNBC is 77%. In contrast, this rate plummets to 14% for those in the advanced stage[3]. Traditional treatment modalities for TNBC include surgery, radiotherapy, and chemotherapy. However, in advanced cases, these treatments face more significant difficulties, which call for a combined-therapy approach[4]. Discovering molecular targets for diagnostic and prognostic purposes is of utmost importance in improving patient survival rates.

Long non-coding RNAs (lncRNAs) are defined as transcripts over 200 nucleotides in length and make up a substantial part of the human transcriptome[5]. Unlike messenger RNAs, lncRNAs are not directly engaged in the process of protein synthesis. Instead, they have regulatory functions in a wide range of biological processes, including chromatin remodeling, regulation of transcription, RNA splicing, and transport[6-9]. Moreover, lncRNAs can function as competing endogenous RNAs (ceRNAs). They can interact with microRNAs (miRNAs), blocking them from interacting with their target messenger RNAs (mRNAs) and thus altering miRNA-mediated gene expression. Additionally, lncRNAs can act as platforms for RNA-protein complexes. These complexes can recruit chromatin-modifying enzymes and transcription factors to modulate the activity of target genes[10].

The lncRNA LINC01232 displays tumor-specific expression profiles and is involved in regulating various cancer-promoting processes. Li et al.[11] discovered that LINC01232 was markedly elevated in pancreatic adenocarcinoma (PAAD) tissues and was correlated with an unfavorable prognosis. LINC01232 was found to recruit EIF4A3, which helped stabilize TM9SF2 mRNA, thus influencing the cancer-promoting characteristics of pancreatic cancer. Chen et al.[12] observed that LINC01232 was highly expressed in gastric cancer and was located mainly in the cytoplasm. When LINC01232 was inhibited, the migration, invasion, and epithelial-mesenchymal transition (EMT) abilities of gastric cancer cells were notably

* Corresponding author.
E-mail address: anjie12024@163.com (J. An).
Doi: http://dx.doi.org/10.14715/cmb/2025.71.7.10

reduced. miR-506-5p was lowly expressed in gastric cancer and served as miR-506-5p sponge to accelerate cell migration and EMT. As a result, the LINC01232/miR-506-5p/PAK1 pathway facilitates the metastasis of gastric cancer cells. However, there is limited research on the role of LINC01232 in TNBC. Consequently, the objective of this research is to explore the function of LINC01232 in TNBC and to investigate its regulatory interaction with the miR-516a-5p/BCL9 pathway. This research aims to offer new perspectives on the development of TNBC and may aid in the creation of more effective therapeutic approaches for TNBC patients.

2. Materials and methods

2.1. General information and reagents

The human breast cancer cell lines, namely HS-578T, HCC1937, and MDA-MB-231, along with the normal breast epithelial cell line MCF-10A, were acquired from the Biological Specimen Bank of the Fourth Hospital of Hebei Medical University. The reagents employed in this research comprised the reverse transcription kit (Cat. No. 4897030001) from Roche, the Lipofectamine 2000 Transfection Reagent (Cat. No. 11668-019) from Invitrogen (located in the USA), and the RIPA lysis buffer (Cat. No. R0010) from Solarbio (based in Beijing, China). To evaluate cell proliferation and gene expression, we made use of the MTS assay kit (Cat. No. G3582) and the Dual-Luciferase Reporter Assay kit (Cat. No. E1910) from Promega, as well as the qRT-PCR kit (Cat. No. 11201ES03) from Yeasen Biologicals. For miRNA extraction, cDNA synthesis, and fluorescence quantification, we utilized the miRcute miRNA Extraction and Isolation Kit (Cat. No. DP501), the miRcute Enhanced miRNA cDNA First Strand Synthesis Kit (Cat. No. KR211), and the miRcute Enhanced miRNA Fluorescence Quantitative Detection Kit (Cat. No. FP411) from Tiangen. The knockdown of LINC01232 and BCL9 was carried out using plasmids (sh-LINC01232 and sh-BCL9) and miR-516a-5p mimics and inhibitors, all of which were obtained from Suzhou GenePharma. Antibodies targeting human BCL9 (Cat. No. ab37304) and GAPDH (Cat. No. ab9485) were procured from Abcam (located in the UK). Primers, including the miR-516a-5p-specific primer (Tiangen MIMAT0002859), were synthesized by Tiangen Biological Co.

The criteria for inclusion were: (1) female with non-specific invasive breast cancer; (2) Negative ER and PR; (3) Negative HER2, which was defined as an immunohistochemistry (IHC) score of 0/1+. For 2+, negative fluorescence in situ hybridization (FISH) results were required; (4) Comprehensive clinical records, including demographic information, tumor-node-metastasis (TNM) staging, treatment plans, and survival data. The exclusion criteria consisted of: (1) History of systemic treatment for breast cancer, for instance, chemotherapy or endocrine therapy; (2) Cases of bilateral breast cancer.

The collected samples were split into two portions. One portion was promptly immersed in liquid nitrogen and then preserved at-80°C for the purpose of RNA extraction and subsequent analysis. The other portion was processed for immunohistochemical assessments.

This research was carried out with the rigorous authorization of the Ethics Committee of Bethune International Peace Hospital (authorization number: 2022-KY-77). All participants provided informed consent, thereby guaranteeing that ethical guidelines were adhered to and the rights of patients were safeguarded.

2.2. Culture and transfection of breast cancer cells

Retrieve the cryopreserved breast cancer cells from the liquid nitrogen reservoir and thaw them rapidly in a 37°C water bath while gently agitating. Introduce the thawed cells into a pre-warmed culture medium (DMEM supplemented with 10% FBS). Gently blend the mixture and then transfer it to culture flasks for cultivation. The incubator conditions were kept at 37°C, with 5% CO_2 and 95% relative humidity. When the cells reached around 80% confluence, they were sub-cultured. The cells were then plated into culture plates to guarantee that they were in the logarithmic growth phase. The plasmids intended for transfection were purified to be endotoxin-free using the Plasmid Extraction Kit. The plasmid and the transfection reagent were combined in accordance with the Lipofectamine 2000 protocol to create the plasmid-transfection reagent complex. Subsequently, add this complex to the cell culture plate and gently agitate to facilitate complete contact between the complex and the cells. Place the plate in the incubator for further culturing. Within 48 hours after transfection, monitor the cellular alterations, document cell growth, and isolate RNA for qRT-PCR to evaluate the transfection efficiency.

2.3. qRT-PCR experimentation

Total RNA was separated from tissue and cell samples utilizing the Trizol methodology. Place the sample tissues or cells into EP tubes and introduce 1 ml Trizol reagent to homogenize and lyse the cells over a 5-minute period. Centrifuge at 12,000 rpm for 15 min at 4°C to precipitate cell debris and proteins. Carefully remove the RNA-containing supernatant to a new EP tube. Introduce 500 µl isopropanol, mix well and incubate at 4°C for 10 min. Centrifuge the mixture to precipitate the RNA, then discard the supernatant and clean the RNA pellet with 75% ethanol. Dry the pellet at 4°C and dissolve it in DEPC-treated water. Assess the concentration and purity of the RNA, document the data, and keep the RNA at -80°C.

Following the directions of the Roche Reverse Transcription Kit, add RNA samples, reverse transcription buffer, enzymes, and primers to PCR reaction tubes. Determination of LINC01232 and BCL9 expression levels by qRT-PCR. The specific primer sequences are presented in Table 1. The qRT-PCR program consisted of: an initial step

Table 1. qRT-PCR primers.

Primer name	Primer sequence
LINC01232	F:5'-TGGAACCGGACTTTCAGAGC-3'
	R:5'-GCTTCTCCGGGTTTTTGCTG-3'
GAPDH	F:5'-AGGTGAAGGTCGGAGTCAACG-3'
	R:5'-AGGGGTCATTGATGGCAACA-3'
U6	F:5'-CTCGCTTCGGCAGCACA-3'
	R:5'-AACGCTTCACGAATTTGCGT-3'
miR-516a-5p	5'-AUCUGGAGGUAAGAAGCACUUU-3'
miR-U6	F:5'-CTCGCTTCGGCAGCACA-3'
BCL9	F:5'-GCCACCACTACCTCTCAACC-3'
	R:5'-CCAGCATTGGTGACTGGACT-3'

F: forward primer; R: reverse primer.

at 95°C for 30 s (pre-denaturation), followed by 40 cycles of 95°C for 15 s (denaturation), 60°C for 30 s (annealing), and 72°C for 30 s (extension). The results were computed using the relative quantification method (2-ΔΔCT), with GAPDH or U6 serving as endogenous controls. Total RNA was extracted from cell lines, TNBC tissues, and adjacent non-cancerous tissues using the miRcute miRNA Extraction and Isolation Kit (DP501). The synthesis of cDNA was carried out using the miRcute Enhanced miRNA cDNA First-Strand Synthesis Kit (KR211). The quantification of miR-516a-5p was achieved with the miRcute Enhanced miRNA Fluorescence Quantification Kit (SYBR Green, FP411). Upstream primers were designed (sequences provided in Table 1), and reverse primers, along with the U6 internal reference primer, were supplied by the kit. The qPCR conditions were as follows: 94°C for 15 min (pre-denaturation), followed by 40 cycles of 94°C for 20 s (denaturation) and 60°C for 34 s (annealing/extension).

2.4. Immunohistochemical analysis

Breast tissue samples were stored in 4% paraformaldehyde, subjected to dehydration, and then embedded in paraffin. The fixed tissue specimens were sliced into sections with a thickness of 4-6 μm, underwent dewaxing, and were treated with ethanol to remove endogenous peroxidase activity. The primary antibody was incubated at 4°C for an overnight period. The secondary antibody, which was linked to a chromogen, was incubated at room temperature for 60 min. DAB was employed for color development, and subsequently, hematoxylin was used for counterstaining. The stained tissues were dehydrated, cleared, and a coverslip was applied using mounting gum. The staining outcomes were qualitatively assessed under a microscope, taking into account the location and intensity of antigen expression.

2.5. Subcellular fractionation and localization studies

RNA was isolated from the nuclear and cytoplasmic compartments of cells using a nuclear/cytoplasmic fractionation kit obtained from Biovision. Breast cancer cells were plated into culture plates and permitted to attain the logarithmic growth phase. The cells were then trypsinized and resuspended in the buffer supplied with the kit. The fractionation columns were utilized to separate the cells into nuclear and cytoplasmic components, with each component being collected in distinct EP tubes. RNA was derived from these components and then reverse-transcribed to cDNA. The quantification of LINC01232 in the cytoplasmic and nuclear components was carried out using qRT-PCR, with GAPDH and U6 serving as the respective controls for the nuclear and cytoplasmic components.

2.6. Cell proliferation assays

MTS Assay: 96-well plate with 1000 breast cancer cells and 100 μl of medium per well. At 0, 24, 48, 72, and 96 hours after plating, add 20 μl of MTS solution to each well and culture for 2 h. The cells metabolized MTS into formazan crystals, and the amount of these crystals was directly proportional to the cell count. The absorbance at 490 nm was determined for each well with a spectrophotometric plate reader. This experiment was performed in triplicate, and the cell proliferation activity was evaluated based on the average absorbance values of each group.

Clone Formation Assay: 6-well plates contain 3000 transfected cells and 2 ml of medium per well. Cell growth was observed on a daily basis during the incubation period. Once visible clones were formed, the culture process was stopped. Cells were rinsed with PBS, stabilised with methanol for 20 min, and then blotted with 1% crystal violet for 20 min. Afterward, the cells were washed with PBS again, air-dried, and clones comprising more than 50 cells were counted under a microscope. This experiment was also carried out in triplicate, and the average number of clones per group was determined.

2.7. Transwell migration and invasion evaluations

For the invasion evaluation, BD Matrigel was diluted at a 1:8 ratio and evenly coated onto the upper chamber surface of the Transwell membrane. Then the gel was incubated at 37°C for 30 min to polymerise into a gel-like matrix. The digested and transfected cells were resuspended with serum-free medium, and 100 μl of 1×10^5 cells was incorporated into the Transwell chambers. In the lower chamber of the Transwell, 700 μl of complete medium enriched with serum was added. The serum acted as a chemoattractant, prompting cell migration from the serum-free environment of the Transwell to the serum-rich one. After 24h, the Transwell inserts were taken out, and the upper chamber was gently cleaned with a cotton swab to remove non-migrated cells. The chamber was then rinsed with PBS and fixed in methanol for 15 min. After that, the cells were coloured with 0.1% crystal violet for 15 min. The number of cells that had moved across the membrane was counted in five random fields under an inverted microscope, and the average was calculated. Note: The Matrigel matrix gel is not utilized in the migration evaluation; all other steps are the same as those in the invasion evaluation.

2.8. Bioinformatics approaches

Within the GEO database, we conducted a search and downloaded TNBC microarray data, specifically acquiring the GSE38959 gene chip dataset. The screening parameters were established to pinpoint genes with a fold change exceeding 2 and a P-value below 0.05. Based on these criteria, we characterized the differentially expressed lncRNAs between TNBC and normal tissues.

Prediction of LINC01232 Interaction with miR-516a-5p: Using Starbase v2.0 (http://starbase.sysu.edu.cn/), we logged into the platform, chose the "RNA-RNA Interaction" option, entered the sequence details of LINC01232 and miR-516a-5p, and started a search to find their binding sites and related information.

miR-516a-5p Target Gene Prediction: By utilizing TargetScan 7.2 (http://www.targetscan.org/) and miRWALK 3.0 (http://zmf.umm.uni-heidelberg.de/apps/zmf/mirwalk2), we visited the respective websites of TargetScan 7.2 or miRWALK 3.0, input the sequence data of miR-516a-5p, examined the list of predicted target genes, and recorded the findings pertaining to BCL9.

2.9. Dual-Luciferase reporter evaluation

A reporter gene vector was planned, created, and introduced into breast cancer cells. After a 48-hour transfection duration, the cells were gathered and lysed. In accordance with the Dual-Luciferase Reporter Assay protocol provided by Promega, the lysate was centrifuged, and the supernatant was moved to the assay plate along

with the necessary reagents to quantify luciferase activity. Then, Stop&Glo Reagent was introduced to determine the control luciferase activity. The relative luciferase activity was computed based on the collected data.

2.10. RNA Immunoprecipitation (RIP) evaluation

Cells are harvested and lysed utilizing RIP lysis buffer, which leads to the release of cellular proteins and RNA. The lysate is then incubated with either a GFP antibody (sourced from Roche) or IgG to bind to the target proteins. Magnetic beads are employed to precipitate the protein-antibody complexes. The precipitated complexes are subsequently washed to eliminate any unbound substances. Following this, RNA is extracted from the proteins via nuclease treatment. The quantity of the isolated RNA is determined by assessing its abundance using qRT-PCR.

2.11. Western Blot (WB) analysis

Cells were lysed in RIPA buffer for a duration of 30 min and then centrifuged at 12,000 rpm for 20 min to obtain the supernatant. The protein concentrations were calculated using the BCA protein assay. An equal quantity (20 μg) of each sample was packed into a 10% SDS-PAGE gel and underwent electrophoresis. Proteins were then attached to the PVDF membrane for 2 hours at a steady current of 200 mA. Following the transfer, block the PVDF membrane with 5% bovine serum albumin for 60 minutes at room temperature. Anti-BCL9 and GAPDH antibodies were added and incubated overnight at 4°C. After being washed with TBST buffer, the secondary antibody was incubated for 1 hour at room temperature. The PVDF membrane was visualized using a gel documentation system, and the grayscale values of the protein bands were assessed using Image J software. The Western blotting for BCL9 protein expression was carried out in triplicate to guarantee reproducibility.

2.12. Statistical analysis

The SPSS (USA) was employed for descriptive statistical analysis. This involved calculating the mean and standard deviation to gain insights into the fundamental characteristics and distribution of the data. Measurement data were presented as Mean ± SD. A t-test was conducted to identify significant differences between the means of the two groups. One-way ANOVA was utilized to assess significant differences among multiple groups, with the LSD method employed for post-hoc pairwise comparisons. Repeated-measures ANOVA was applied to the results of the MTS experiment. The statistical data from BCL9 immunohistochemistry, which were categorical in nature, were analyzed using the chi-square test for four-cell contingency tables. Spearman's rank correlation was used to examine the correlation between LINC01232, miR-516a-5p, and BCL9. GraphPad Prism 6.0 software was used to process the experimental data. The results were exported as figures or tables and were cited and interpreted in the thesis. $P \leq 0.05$ was regarded as statistically significant.

3. Results

3.1. Upregulation of LINC01232 in TNBC and its correlation with clinicopathological characteristics

Microarray data related to TNBC were obtained from the GEO database, and the GSE38959 dataset was chosen for analysis. We pinpointed genes that were notably up-or down-regulated in TNBC tissues by applying the standard of log|FC| > 2 and $P<0.05$. LINC01232 expression was notably upregulated by 2.593-fold in TNBC, as demonstrated by volcano and heatmap analyses (Fig. 1). An analysis using the GEPIA database, which is founded on TCGA and GTEx data, verified the significant upregulation of LINC01232 in TNBC tissues. qRT-PCR analysis revealed that the expression of LINC01232 in TNBC tissues was obviously higher than that in the neighbouring normal tissues (0.797±0.449 vs 2.524±1.099, t=11.273, $P<0.001$). Moreover, LINC01232 expression levels were significantly linked to lymph node metastasis and TNM staging (2.189±1.041 vs 3.012±1.164, t=2.741, $P=0.008$; 2.018±1.006 vs 2.866±1.170, t=2.222, $P=0.030$). LINC01232 expression differed noticeably between normal breast cells and breast cancer cells, with expression levels of 1.003±0.121, 1.120±0.085, 1.343±0.140, and 2.056±0.029. LINC01232 expression was remarkably increased in breast cancer cells (F=59.585, $P<0.001$). Further pairwise comparisons confirmed that LINC01232 expression was remarkably higher in the HS-578T, HCC1937, and MDA-MB-231 cell lines compared to normal cells ($P=0.047$, $P=0.004$, $P<0.001$). These results suggest that LINC01232 may play an oncogenic role in TNBC, and its high expression may be correlated with disease progression and malignancy.

The Critical Role of LINC01232 in the Malignant Progression of Breast Cancer Cells

To thoroughly evaluate the biological function of LINC01232 in breast cancer cells, a knockdown experiment was performed in the HS-578T cell line. The expression of LINC01232 in the control and knockdown

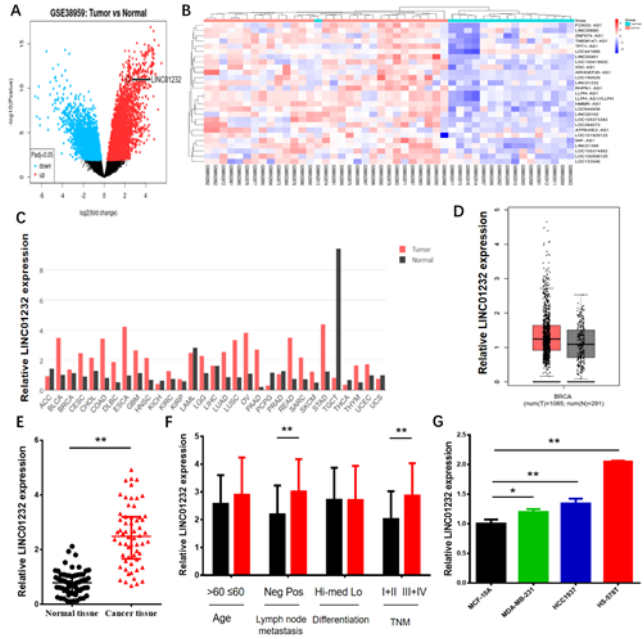

Fig. 1. High expression of LINC01232 in breast cancer. Figures a and b show the differentially expressed genes predicted in breast cancer from the GEO database, respectively; Figures c and d display the expression of LINC01232 in breast cancer tissues from the GEPIA database, respectively; Figure e presents the detection of 60 pairs of breast cancer specimens and normal samples using qRT-PCR technology; Figure f shows the expression of LINC01232 in different subgroups; Figure g shows the expression levels of LINC01232 in breast cancer cell lines detected by qRT-PCR.

groups was 0.974±0.064, 0.412±0.044, 0.213±0.031, and 0.344±0.034, respectively. The knockdown group showed discernable lower LINC01232 expression (F=167.157, *P*<0.001). Subsequent pairwise comparisons indicated that sh-LINC01232-1 to sh-LINC01232-4 all had reduced expression compared to the control (*P*<0.001 for all). Among them, sh-LINC01232-2 demonstrated the highest knockdown efficiency and was chosen for further experiments. The MTS assay was initially employed to assess the impact of LINC01232 knockdown on breast cancer cell proliferation. It showed a significant effect (F=884.428, *P*<0.001) and an interaction between subgroups and time points (F=54.276, *P*<0.001). Cell proliferation in the LINC01232 knockdown group was remarkably reduced at 72 and 96 hours compared to the control group (1.246±0.030 vs 1.012±0.043, t=8.933, *P*<0.001; 1.888±0.063 vs 1.253±0.138, t=8.378, *P*<0.001). Clone formation assays confirmed that the LINC01232 knockdown group had a noticeably lower number of clones than the control group (850.000±20.075 vs 344.333±14.572, t=35.308, *P*<0.001, Fig. 2a, b), thus establishing LINC01232's role in promoting breast cancer cell proliferation. A Transwell assay revealed that LINC01232 knockdown significantly reduced the number of migrating and invading cells compared to the control group (539.000±11.136 vs 242.333±6.110, t=40.455, *P*<0.001; 640.667±9.292 vs 217.000±12.127, t=48.039, *P*<0.001, Fig. 2c, d, e, f), emphasizing the essential role of LINC01232 in the biological behaviour of breast cancer cells.

3.2. LINC01232 modulates miR-516a-5p expression

Nuclear-cytoplasmic separation experiments showed that LINC01232 was primarily situated in the cytoplasm, implying a regulatory function as ceRNA. By using the bioinformatics tool StarBase v2.0, we predicted a base-complementary binding site (GAGCU) between LINC01232 and miR-516a-5p. Luciferase assays in breast cancer cells with miR-516a-5p mimics showed a significant reduction in luciferase activity in the pmirGLO-LINC01232-WT group (1.140±0.070 vs 0.347±0.060, t=14.875, *P*<0.001), while the mutant group was unchanged. RIP assays revealed a significant increase in miR-516a-5p enrichment after LINC01232 overexpression (0.948±0.185 vs 5.953±1.453, t =-5.915, *P*=0.004). qRT-PCR of miR-516a-5p expression in breast cancer tissues showed significantly lower expression compared to normal tissues (0.941±0.553 vs 0.615±0.302, t=3.999, *P*<0.001). Furthermore, miR-516a-5p expression levels were significantly different in relation to lymph node metastasis and TNM staging (0.543±0.287 vs 0.740±0.293, t =-2.540, *P*=0.014; 0.545±0.269 vs 0.927±0.244, t =-4.322, *P*<0.001). A remarkable negative relationship was observed between the expression level of miR-516a-5p and LINC01232 (R =-0.293, *P*=0.023), indicating that LINC01232 binds to miR-516a-5p and suppresses its function.

3.3. Tumor-suppressive effects of miR-516a-5p in TNBC

To evaluate the functional role of miR-516a-5p in breast cancer cells, overexpression and knockdown experiments were conducted using the MDA-MB-231 cell line. qRT-PCR showed different expression levels of miR-516a-5p in the control, mimic, and inhibitor groups, with values of 0.951±0.233, 2.335±0.207, and 0.356±0.061, respectively. Transfection of miR-516a-5p mimics and inhibitors in MDA-MB-231 cells resulted in significant changes in their expression (F=92.271, *P*<0.001). The paired comparisons established that marked differences from the control group for both the mimic (*P*<0.001) and inhibitor groups (*P*=0.007). MTS assay results demonstrated a significant impact on cell proliferation (F=8241.357, *P*<0.001) and an interaction between subgroups and time points (F=227.229, *P*<0.001). Specifically, the miR-516a-5p mimic groups showed a markedly decrease in proliferation at 72 and 96 hours compared to the control group (1.439±0.039 vs 1.232±0.026, t=8.909, *P*<0.001; 2.261±0.078 vs 1.815±0.059, t=9.456, *P*<0.001), while the inhibitor group showed increased

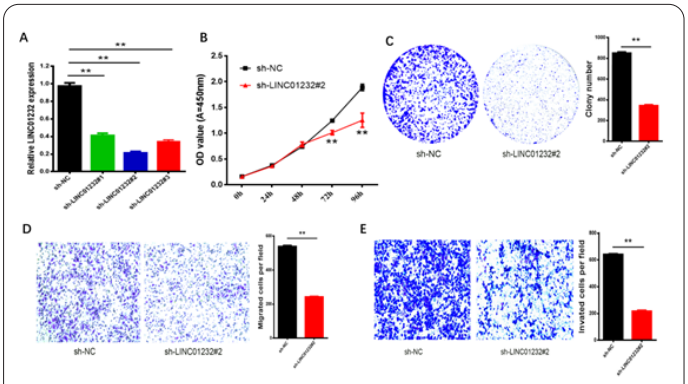

Fig. 2. The effects of LINC01232 on the proliferation, migration, and invasion abilities of breast cancer cells. Figure a shows the detection of LINC01232 expression in breast cancer cells transfected with sh-LINC01232 using qRT-PCR technology; Figure b presents the proliferation ability of breast cancer cells with sh-LINC01232 as shown by the MTS assay; Figure c displays the number of clones formed by breast cancer cells transfected with sh-LINC01232 in the clone formation assay; Figure d shows the migration ability of breast cancer cells transfected with sh-LINC01232 in the Transwell assay; Figure e presents the invasion ability of breast cancer cells transfected with sh-LINC01232 detected by the Transwell assay.

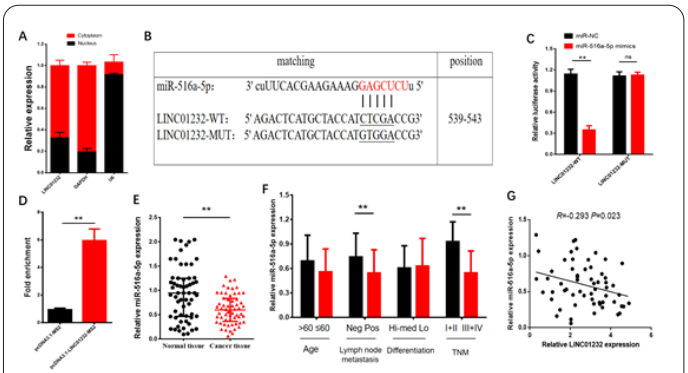

Fig. 3. The interaction between LINC01232 and miR-516a-5p in breast cancer. Figure a shows the nuclear-cytoplasmic localization of LINC01232 in the breast cancer cell line HS-578T. Figure b presents the binding sites between the LINC01232 sequence and miR-516a-5p analyzed by bioinformatics. Figure c displays the binding activity between LINC01232 and miR-516a-5p shown by the dual-luciferase reporter assay. Figure d presents the binding relationship between LINC01232 and miR-516a-5p detected by the RIP assay. Figure e shows the expression of miR-516a-5p in breast cancer tissues as revealed by qRT-PCR. Figure f presents the expression levels of miR-516a-5p among different subgroups. Figure g shows the association between the expression levels of miR-516a-5p and LINC01232 in TNBC samples through correlation analysis.

proliferation (1.439±0.039 vs 1.792±0.010, t =-17.688, *P*<0.001; 2.261±0.078 vs 2.925±0.053, t =-14.087, *P*<0.001). Clone formation assays further supported these findings. The miR-516a-5p mimic group showed a dramatic reduction in clone numbers (435.000±21.166 vs 851.333±13.577), and the inhibitor group showed an increase (1181.667±30.436 vs 851.333±13.577) (F=808.349, *P*<0.001). Pairwise comparisons confirmed dramatic differences from the control group for both the mimic (*P*<0.001) and inhibitor groups (*P*<0.001) (Fig. 3a, b, c). Transwell assays indicated that the miR-516a-5p mimic groups had a significantly lower number of migrated cells compared to the control group (181.000±4.000 vs 376.333±19.604), while the inhibitor group had an increased number of migrated cells (575.000±19.078 vs 376.333±19.604) (F=456.989, *P*<0.001). Pairwise comparisons confirmed dramatic differences from the control group for both the mimic (*P*<0.001) and inhibitor groups (*P*<0.001) (Fig. 3d, e, f). Similarly, the number of invaded cells was significantly lower in the miR-516a-5p mimic group (168.333±6.658 vs 28.333±3.055) and higher in the inhibitor group (620.333±12.662 vs 28.333±3.055) (F=2209.121, *P*<0.001). Pairwise comparisons confirmed dramatic differences from the control group for both the mimic (*P*<0.001) and inhibitor groups (P<0.001) (Fig. 3g, h, i). These results collectively indicate that miR-516a-5p plays a tumor-suppressive role in TNBC.

3.4. BCL9 as a downstream molecule of miR-516a-5p

Bioinformatics tools such as TargetScan and starBase suggested that BCL9 could be a potential target gene of miR-516a-5p. HS-578T cells were co-transfected with wild or mutant pmirGLO-BCL9 vectors along with miR-516a-5p mimics or NC. Dual luciferase reporter gene assay revealed a remarkable reduction in luciferase activity in the pmirGLO-BCL9-WT group after miR-516a-5p mimic treatment (1.160±0.108 vs 0.273±0.065, t=12.167, *P*<0.001), while there was no noticeable change in mutant vector activity (*P*>0.05). This indicates that miR-516a-5p binds to the 3'UTR of BCL9 through base-complementary pairing. GEPIA analysis revealed that BCL9 mRNA was noticeably higher in TNBC tissues. Similarly, UALCAN results indicated that BCL9 protein was discernibly elevated in TNBC tissues. qRT-PCR confirmed that BCL9 mRNA expression in TNBC tissues was noticeably higher (2.141±0.984 vs 0.905±0.447, t=8.859, *P*<0.001), with statistically noticeable differences in lymph node metastasis and TNM staging (1.714±0.712 vs 2.309±1.014, t =-2.424, *P*=0.019; 0.971±0.197 vs 2.404±0.894, t =-5.256, *P*<0.001). Immunohistochemistry detected higher BCL9 protein expression in TNBC tissues (48/60 (80%) vs 9/60 (15%), X^2=50.827, *P*<0.001, Fig. 4). BCL9 mRNA expression was negatively correlated with miR-516a-5p (R=-0.394, *P*=0.002) and positively correlated with LINC01232 (R=0.303, *P*=0.019), suggesting that BCL9 is a direct target of miR-516a-5p.

The Combined Impact of LINC01232 and miR-516a-5p on Breast Cancer Progression

We constructed sh-LINC01232 and miR-516a-5p inhibitor plasmids and assessed the expression of BCL9 mRNA and protein using qRT-PCR and WB analysis. qRT-PCR experiments showed significant differences in BCL9 mRNA expression levels among the sh-NC, sh-LINC01232, and sh-LINC01232 plus miR-516a-5p inhibitor co-transfected groups (1.020±0.066 vs 0.346±0.105 vs 0.910±0.085, F=52.009, *P*<0.001). Silencing LINC01232 led to a marked decrease in BCL9 expression (*P*<0.001), while co-transfection with the miR-516a-5p inhibitor partially restored BCL9 expression (*P*=0.173). WB results supported these findings regarding BCL9 protein expression. MTS assays detected significant differences in breast cancer cell proliferation among the three groups (F=4412.680, *P*<0.001), with an interaction between groups and time points (F=64.100, *P*<0.001). Silencing LINC01232 at 72 and 96 hours obvious suppressed breast cancer cell proliferation (1.834±0.073 vs 1.644±0.060, t=4.011, *P*=0.007; 2.844±0.104 vs 2.045±0.046, t=13.993, *P*<0.001), and co-transfection partially recovered the proliferative capacity (1.834±0.073 vs 1.931±0.085, t =-1.734, *P*=0.134; 2.844±0.104 vs 2.915±0.076, t =-1.091, *P*=0.317). Clone formation assays demonstrated significant differences in clone numbers among the sh-NC, sh-LINC01232, and sh-LINC01232 plus miR-516a-5p inhibitor co-transfected groups (956.667±22.368 vs 279.667±14.364 vs 961.33±29.092, F=891.520, *P*<0.001). Silencing LINC01232 inhibited breast cancer cell proliferation (*P*<0.001), and co-transfection restored it to some degree (*P*=0.810, Fig. 5a, b, c). Transwell experiments to evaluate the effects of LINC01232 and miR-516a-5p on breast cancer cell migration and invasion revealed remarkable differences in the number of migrated and invaded cells among the groups (migrated: 528.000±7.937 vs 209.333±6.110 vs 529.333±6.658, F=2114.691, *P*<0.001; invaded: 607.667±6.506 vs 319.333±7.095 vs 720.333±19.553, F=810.413, *P*<0.001). Silencing LINC01232 noticeably reduced migration and invasion (*P*<0.001 for both), and co-transfection restored these abilities (migration: P=0.822, invasion: *P*<0.001, Fig. 5d, e, f, g, h, i). These results suggest that LINC01232 and miR-516a-5p jointly modulate BCL9 expression and the proliferation, migration, and invasion of breast cancer cells, emphasizing the LINC01232/miR-516a-5p axis as a crucial factor in TNBC development and a potential therapeutic target. Results showed that LINC01232 and

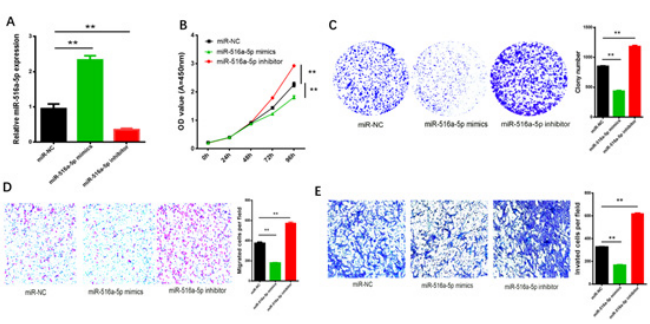

Fig. 4. The effects of miR-516a-5p on the biological behavior of breast cancer cells. Figure a shows the transfection efficiency of miR-516a-5p mimics or inhibitors in breast cancer cells detected by qRT-PCR. Figure b presents the proliferation ability of breast cancer cells with miR-516a-5p mimics and inhibitors as shown by the MTS assay. Figure c displays the effect of miR-516a-5p on the proliferation of breast cancer cells detected by the clone formation assay. Figure d shows the migration ability of breast cancer cells transfected with miR-516a-5p mimics and inhibitors in the Transwell assay. Figure e presents the invasion ability of breast cancer cells affected by miR-516a-5p in the Transwell invasion assay.

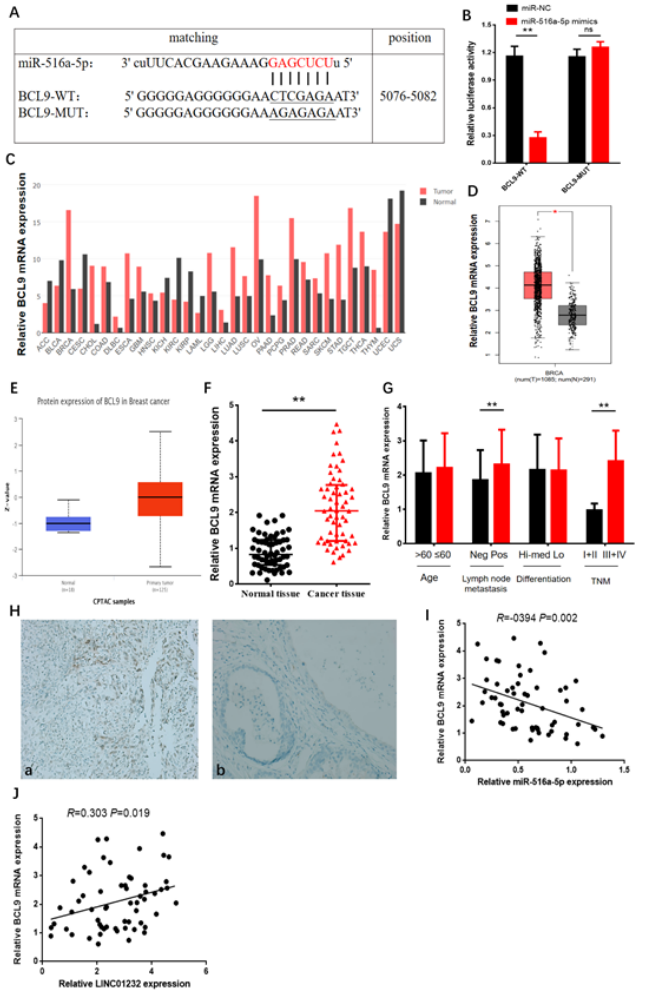

Fig. 5. BCL9 serves as a target gene of miR-516a-5p and is regulated by LINC01232. (a): the binding sites of miR-516a-5p on the 3'UTR of BCL9 predicted by bioinformatics methods. **(b):** the binding sites between miR-516a-5p and BCL9 demonstrated by the luciferase reporter assay. **(c, d, and e):** the expression levels of BCL9 in TNBC tissues from the GEPIA and UALCAN databases, respectively. **(f):** the expression levels of BCL9 in TNBC tissues detected by qRT-PCR. **(g):** the expression of BCL9 among different subgroups. **(h):** the expression levels of BCL9 protein in TNBC tissues revealed by immunohistochemical staining. **(i):** the association between the expression levels of miR-516a-5p and BCL9 in TNBC samples through association analysis. **(j):** the association between the expression levels of LINC01232 and BCL9.

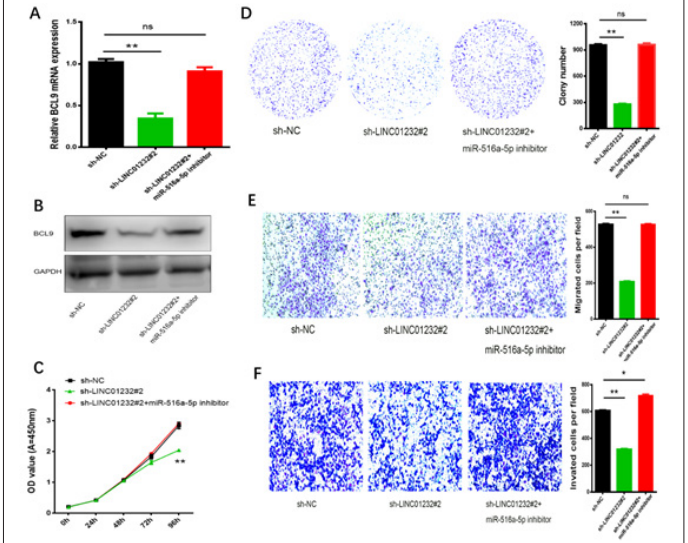

Fig. 6. LINC01232 and miR-516a-5p jointly regulate BCL9 expression and breast cancer progression. (a): shows that LINC01232 upregulates BCL9 mRNA levels by inhibiting miR-516a-5p expression, as revealed by qRT-PCR. **(b):** presents that LINC01232 upregulates BCL9 protein levels by inhibiting miR-516a-5p expression, as shown by the WB results. **(c and d)** demonstrate the effects of co-transfecting LINC01232 and miR-516a-5p on the proliferation of breast cancer cells through the MTS and clone formation assays, respectively. **(e and f):** further reveal the effects of co-transfecting LINC01232 and miR-516a-5p on the migration and invasion abilities of breast cancer cells through the Transwell migration and invasion assays, respectively.

miR-516a-5p jointly regulate BCL9 expression and breast cancer progression (Figure 6).

4. Discussion

Breast cancer remains the most common malignant tumour in women worldwide, posing a substantial threat to their physical and mental well-being[13]. The most recent GLOBOCAN 2020 statistics reveal that breast cancer has exceeded lung cancer as the most prevalent cancer in the world[14]. Breast cancer can be divided into subtypes based on biomarkers such as ER, PR, HER2 and Ki67. These subtypes encompass Luminal A, Luminal B, HER2-overexpressing, TNBC, and Normal Breast-like[15]. Notably, TNBC is marked by its lack of response to traditional endocrine and antibody treatments, which results in high recurrence and mortality rates[16]. Discovering molecular targets for diagnostic and prognostic purposes is of utmost importance in enhancing patient survival rates.

LncRNAs are RNA molecules over 200 nucleotides in length that do not encode proteins and are essential for regulating gene expression[17, 18]. LncRNAs, like LINC01232, are engaged in tumourigenesis and progression. They affect the growth, proliferation, and migration of tumor cells and are linked to drug resistance, recurrence, and prognosis in cancers[19, 20]. Zhang et al.[21] observed elevated LINC01232 expression in lung squamous cell carcinoma (LUSC). Further research indicated that LINC01232 promotes LUSC progression by regulating miR-181a-5p and SMAD2 signaling. Liu et al.[22] discovered that LINC01232 expression in clear cell renal carcinoma (ccRCC) tissues and cells could predict patient prognosis. Silencing LINC01232 inhibited renal carcinoma cell proliferation, migration, and invasion by modulating miR-204-5p and RAB22A expression. Our group's initial results from tissue microarray technology and qRT-PCR analysis showed notably high LINC01232 expression in TNBC tissues, which was correlated with patients' clinicopathological data. Functional experiments demonstrated that LINC01232 significantly promotes breast cancer cell proliferation, migration, and invasion, indicating its oncogenic role in TNBC development and progression.

Competitive endogenous RNAs (ceRNAs) are endogenous RNA molecules that can bind to miRNAs and regulate miRNA-mediated silencing of target genes through competitive mechanisms[23]. Our nuclear-cytoplasmic isolation experiments revealed that LINC01232 is mainly expressed in the cytoplasm, suggesting its potential role as a ceRNA. Starbase v2.0 predicted that LINC01232 could bind to miR-516a-5p, miR-429, and miR-936, and LINC01232 noticeably downregulated miR-516a-5p expression. miR-516a-5p has shown differential expres-

sion in various malignancies, including breast cancer. Ye et al.[24] found that reduced miR-516a-5p expression in non-small cell lung cancer (NSCLC) tissues correlated with age, pathological stage, and tumor size, and was an independent prognostic factor for tumor recurrence in NSCLC patients. miR-516a-5p exerts tumor-suppressive effects by targeting HIST3H2A in NSCLC cells. Zou et al.[25] reported that circMYC was positively related to poor prognosis in acute myeloid leukemia patients. Knocking down circMYC reduces cell viability and OCR but extends apoptosis, and a similar trend was observed with miR-516a-5p overexpression. Mechanistically, reducing circMYC could inhibit AML progression by miR-516a-5p/AKT3, providing a new therapeutic target for AML treatment. Our group found that miR-516a-5p inhibits breast cancer cell proliferation, migration, and invasion, which is in contrast to the pro-cancer effects of LINC01232. RIP and luciferase assays confirmed a base-complementary binding site between LINC01232 and miR-516a-5p, suggesting that LINC01232 may affect TNBC cell biology by modulating miR-516a-5p expression.

Moreover, bioinformatics tools such as TargetScan and starBase forecasted BCL9, RASSF9, and HIST3H2A as the target genes of miR-516a-5p. It was discovered that miR-516a-5p noticeably downregulates BCL9 expression. BCL9, which is situated on human chromosome 1q21[26], serves as a co-activator in the Wnt signaling pathway[27], It has been linked to multiple cancers, including colorectal cancer, hepatocellular carcinoma, and lung adenocarcinoma[28-30]. Our research showed that BCL9 is highly expressed in TNBC tissues, and its expression level is closely linked to LINC01232 and miR-516a-5p. LINC01232, functioning as a ceRNA, can counteract the inhibitory impact of miR-516a-5p on its target mRNAs, thus facilitating breast cancer cell proliferation, migration, and invasion. BCL9 is a downstream target of the LINC01232/miR-516a-5p axis and is involved in the malignant progression of TNBC.

In conclusion, LINC01232 is overexpressed in breast cancer. It operates by competitively binding to miR-516a-5p in the cytoplasm, which hinders miR-516a-5p's inhibitory effect on BCL9 and triggers BCL9 translation. The discovery of this mechanism provides fresh perspectives and potential therapeutic targets for breast cancer treatment.

Data availability statement

Reasonable requests can be made to the corresponding author to obtain the datasets generated and/or analyzed during this research. All relevant data are encompassed in the manuscript and its supplementary materials.

Acknowledgments

We would like to express our sincere gratitude to the Free Statistics team, based in Beijing, China, for providing technical support along with practical tools for data analysis and visualization.

Funding

This study was supported by the Medical Science Research Program Project of Hebei Provincial Health and Wellness Commission (No. 20231315).

Institutional review board statement

This research was carried out in line with the ethical guidelines set by the Ethics Committee of Bethune International Peace Hospital (approval number: 2022-KY-77).

Consent for publication

All authors have reviewed and approved the manuscript for publication.

Disclosure statement

No potential conflict of interest was reported by the authors.

Author contributions

Wei Liu (the primary author) was responsible for project management, conceptual development, data organization, methodology design, software utilization, and the initial drafting, review, and revision of the manuscript.

Yunfeng Niu contributed to project administration, conceptualization, data curation, methodology formulation, software application, and the original drafting of the manuscript.

Jie An was involved in validation processes, manuscript review and editing, visualization tasks, supervisory duties, and conducted relevant investigations.

Supplementary information

Supplementary file: It includes supplementary findings and the outcomes of sensitivity analyses.

References

1. Yan S, Wang J, Chen H, Zhang D, Imam M (2023) Divergent features of ERβ isoforms in triple negative breast cancer: progress and implications for further research. Front Cell Dev Biol 11: 1240386. doi: 10.3389/fcell.2023.1240386
2. Alsamri H, Al Dhaheri Y, Iratni R (2023) Targeting Triple-Negative Breast Cancer by the Phytopolyphenol Carnosol: ROS-Dependent Mechanisms. Antioxidants (Basel) 12 (7). doi: 10.3390/antiox12071349
3. Nayak V, Patra S, Singh KR, Ganguly B, Kumar DN, Panda D, Maurya GK, Singh J, Majhi S, Sharma R, Pandey SS, Singh RP, Kerry RG (2023) Advancement in precision diagnosis and therapeutic for triple-negative breast cancer: Harnessing diagnostic potential of CRISPR-cas & engineered CAR T-cells mediated therapeutics. Environ Res 235: 116573. doi: 10.1016/j.envres.2023.116573
4. Yin L, Duan JJ, Bian XW, Yu SC (2020) Triple-negative breast cancer molecular subtyping and treatment progress. Breast Cancer Res 22 (1): 61. doi: 10.1186/s13058-020-01296-5
5. Su T, Liu J, Zhang N, Wang T, Han L, Wang S, Yang M (2023) New insights on the interplays between m(6)A modifications and microRNA or lncRNA in gastrointestinal cancers. Front Cell Dev Biol 11: 1157797. doi: 10.3389/fcell.2023.1157797
6. Amicone L, Marchetti A, Cicchini C (2023) The lncRNA HOTAIR: a pleiotropic regulator of epithelial cell plasticity. J Exp Clin Cancer Res 42 (1): 147. doi: 10.1186/s13046-023-02725-x
7. Pant T, Uche N, Juric M, Bosnjak ZJ (2023) Clinical Relevance of lncRNA and Mitochondrial Targeted Antioxidants as Therapeutic Options in Regulating Oxidative Stress and Mitochondrial Function in Vascular Complications of Diabetes. Antioxidants (Basel) 12 (4). doi: 10.3390/antiox12040898
8. Zhang Q, Wang C, Yang Y, Xu R, Li Z (2023) LncRNA and its

role in gastric cancer immunotherapy. Front Cell Dev Biol 11: 1052942. doi: 10.3389/fcell.2023.1052942
9. Li K, Wang Z (2023) lncRNA NEAT1: Key player in neurodegenerative diseases. Ageing Res Rev 86: 101878. doi: 10.1016/j.arr.2023.101878
10. Xu J, Wang X, Zhu C, Wang K (2022) A review of current evidence about lncRNA MEG3: A tumor suppressor in multiple cancers. Front Cell Dev Biol 10: 997633. doi: 10.3389/fcell.2022.997633
11. Li Q, Lei C, Lu C, Wang J, Gao M, Gao W (2019) LINC01232 exerts oncogenic activities in pancreatic adenocarcinoma via regulation of TM9SF2. Cell Death Dis 10 (10): 698. doi: 10.1038/s41419-019-1896-3
12. Chen G, Liao J, Xu Y, Chen Y, Li J, Bu G, Li Q (2022) LINC01232 Promotes Metastasis and EMT by Regulating miR-506-5p/PAK1 Axis in Gastric Cancer. Cancer Manag Res 14: 1729-1740. doi: 10.2147/cmar.S352081
13. Wooten J, Mavingire N, Damar K, Loaiza-Perez A, Brantley E (2023) Triumphs and challenges in exploiting poly(ADP-ribose) polymerase inhibition to combat triple-negative breast cancer. J Cell Physiol 238 (8): 1625-1640. doi: 10.1002/jcp.31015
14. Ozyurt R, Ozpolat B (2023) Therapeutic Landscape of AXL Receptor Kinase in Triple-Negative Breast Cancer. Mol Cancer Ther 22 (7): 818-832. doi: 10.1158/1535-7163.Mct-22-0617
15. Torres Quintas S, Canha-Borges A, Oliveira MJ, Sarmento B, Castro F (2024) Special Issue: Nanotherapeutics in Women's Health Emerging Nanotechnologies for Triple-Negative Breast Cancer Treatment. Small 20 (41): e2300666. doi: 10.1002/smll.202300666
16. Guo J, Hu J, Zheng Y, Zhao S, Ma J (2023) Artificial intelligence: opportunities and challenges in the clinical applications of triple-negative breast cancer. Br J Cancer 128 (12): 2141-2149. doi: 10.1038/s41416-023-02215-z
17. Hong Y, Zhang Y, Zhao H, Chen H, Yu QQ, Cui H (2022) The roles of lncRNA functions and regulatory mechanisms in the diagnosis and treatment of hepatocellular carcinoma. Front Cell Dev Biol 10: 1051306. doi: 10.3389/fcell.2022.1051306
18. Yang J, Li Z, Wang L, Yun X, Zeng Y, Ng JPL, Lo H, Wang Y, Zhang K, Law BYK, Wong VKW (2022) The role of non-coding RNAs (miRNA and lncRNA) in the clinical management of rheumatoid arthritis. Pharmacol Res 186: 106549. doi: 10.1016/j.phrs.2022.106549
19. Badmalia MD, Sette Pereira H, Siddiqui MQ, Patel TR (2022) A comprehensive review of methods to study lncRNA-protein interactions in solution. Biochem Soc Trans 50 (5): 1415-1426. doi: 10.1042/bst20220604
20. Abd El Fattah YK, Abulsoud AI, AbdelHamid SG, Hamdy NM (2022) Interactome battling of lncRNA CCDC144NL-AS1: Its role in the emergence and ferocity of cancer and beyond. Int J Biol Macromol 222 (Pt B): 1676-1687. doi: 10.1016/j.ijbiomac.2022.09.209
21. Zhang D, Hua M, Zhang N (2023) LINC01232 promotes lung squamous cell carcinoma progression through modulating miR-181a-5p/SMAD2 axis. Am J Med Sci 365 (4): 386-395. doi: 10.1016/j.amjms.2022.12.014
22. Liu Q, Lei C (2021) LINC01232 serves as a novel biomarker and promotes tumour progression by sponging miR-204-5p and upregulating RAB22A in clear cell renal cell carcinoma. Ann Med 53 (1): 2153-2164. doi: 10.1080/07853890.2021.2001563
23. Zhao Q, Cheng J, Gao A, Wang J, Lu H, Jiang S, Li X, Ni J, Dong W, Lai S, Gong J, Zhu H, Liang Y (2023) Duodenal-Jejunal bypass improves metabolism and re-models extra cellular matrix through modulating ceRNA network. Genomics 115 (6): 110744. doi: 10.1016/j.ygeno.2023.110744
24. Ye XY, Xu L, Lu S, Chen ZW (2019) MiR-516a-5p inhibits the proliferation of non-small cell lung cancer by targeting HIST3H2A. Int J Immunopathol Pharmacol 33: 2058738419841481. doi: 10.1177/2058738419841481
25. Zou X, Jiang M (2021) CircMYC regulates the mitochondrial respiration and cell viability via miR-516a-5p/AKT3 axis in acute myeloid leukemia. Am J Transl Res 13 (9): 10112-10126. doi:
26. Van Outersterp I, Hormann FM, Hoogkamer AQ, Boeree A, Van den Broek SA, Den Boer ML, Boer JM (2023) Characterization of a novel MEF2D-BCL9 fusion-positive acute lymphoblastic leukemia cell line. Haematologica 108 (10): 2859-2864. doi: 10.3324/haematol.2022.281712
27. Zhang X, Zhang R, Hao J, Huang X, Liu M, Lv M, Su C, Mu YL (2022) miRNA-122-5p in POI ovarian-derived exosomes promotes granulosa cell apoptosis by regulating BCL9. Cancer Med 11 (12): 2414-2426. doi: 10.1002/cam4.4615
28. Liu D, Chen C, Cui M, Zhang H (2021) miR-140-3p inhibits colorectal cancer progression and its liver metastasis by targeting BCL9 and BCL2. Cancer Med 10 (10): 3358-3372. doi: 10.1002/cam4.3840
29. Huge N, Sandbothe M, Schröder AK, Stalke A, Eilers M, Schäffer V, Schlegelberger B, Illig T, Vajen B, Skawran B (2020) Wnt status-dependent oncogenic role of BCL9 and BCL9L in hepatocellular carcinoma. Hepatol Int 14 (3): 373-384. doi: 10.1007/s12072-019-09977-w
30. Rao X, Liu X, Liu N, Zhang Y, Zhang Z, Zhou L, Han G, Cen R, Shi N, Zhu H, Gong H, Huang C, Ji Q, Li Q (2021) Long noncoding RNA NEAT1 promotes tumorigenesis in H. pylori gastric cancer by sponging miR-30a to regulate COX-2/BCL9 pathway. Helicobacter 26 (6): e12847. doi: 10.1111/hel.12847